Magnetic Trapping of an Ultracold Gas of Polar Molecules

D. J. McCarron, M. H. Steinecker, Y. Zhu, and D. DeMille

Magnetic Trapping of an Ultracold Gas of Polar Molecules

D. J. McCarron,* M. H. Steinecker, Y. Zhu, and D. DeMille

Department of Physics, Yale University, PO Box 208120, New Haven, Connecticut 06520, USA

We demonstrate the efficient transfer of molecules from a magneto-optical trap (MOT) into a conservative magnetic quadrupole trap. Our scheme begins with a blue-detuned optical molasses to cool SrF molecules to $\approx 50~\mu$K. Next, we optically pump the molecules into a strongly-trapped sublevel. This two-step process reliably transfers $\approx 40\%$ of the molecules initially trapped in the MOT into a single quantum state in the magnetic trap. Once loaded, the molecule cloud is compressed by increasing the magnetic field gradient. We observe a magnetic trap lifetime of over 1 s. This opens a promising new path to study ultracold molecular collisions, and potentially to produce quantum-degenerate molecular gases via sympathetic cooling with co-trapped atoms.

In the last decade, there has been great progress in the production of ultracold polar molecules, beginning with techniques to assemble molecules from pre-cooled alkali atoms [1–4]. These efforts have been motivated by the proposed applications for ultracold molecules in precision measurement [5–7], quantum information [8–10] and quantum simulation [11], and ultracold chemistry [12]. For many of these applications, it is critical to use a sample with high phase-space density (PSD) [13].

Recently, techniques for direct laser cooling [14] and magneto-optical trapping of molecules [15–17] have been developing rapidly and are being pursued as an alternate route to produce ultracold gases of polar molecules. There have been steady improvements in the density and temperature achieved via these methods [17–19], but the accessible PSDs remain modest compared to those of their atomic counterparts. The success of sympathetic cooling techniques for increasing the PSD of atomic samples [20, 21] provides inspiration for the pursuit of similar techniques for molecules. The first step towards implementing these techniques is to load molecules into a conservative trap.

The first magnetic trapping of a molecule was reported in Ref. [22], using superconducting coils in a cryogenic buffer gas cell. Since then, several other experiments have observed magnetic [23, 24], electrostatic [25], or mixed magnetic/electric [26, 27] conservative trapping of directly-cooled molecules. However, in these experiments the temperature of the molecular cloud was always $\gtrsim 400~\mu$K, and typically $\gg 1$ mK. Here, we report magnetic trapping of molecules laser-cooled to temperatures below 100 μK. In this temperature regime, magnetic trapping of laser-cooled atoms with densities sufficient for sympathetic cooling of other species (assuming typical cross-species elastic collision cross-sections [28], as expected [29–33]) is routine [34–36]. Hence, our result opens a straightforward pathway to sympathetic cooling of polar molecules.

The magnetic quadrupole trap (MQT) provides substantial trap depth, large trapping volume, and tight confinement. The limitations of an MQT, including Majorana spin-flip losses [37] and two-body inelastic collisions (due to inability to confine the absolute ground state), are not expected to arise here given the densities ($\lesssim 10^6$ cm^{-3}) and temperatures ($\sim 50~\mu$K) presently accessible via molecular laser cooling and trapping. This makes the MQT an excellent choice to realize the efficient transfer of molecules from a magneto-optical trap (MOT) into a conservative trap.

Here, we demonstrate and characterize the transfer of SrF molecules from a radio-frequency (RF) MOT into an MQT. We apply sub-Doppler cooling followed by optical pumping (OP) to reliably transfer $\approx 40\%$ of the molecules initially trapped in the RF MOT into a single quantum state in the MQT. Once in the MQT, we increase the field gradient to compress the trapped cloud, as is typically done with atomic samples to accelerate evaporative and/or sympathetic cooling (see, e.g., Ref. [38]). Finally, we demonstrate a trap lifetime in excess of 1 s. These conditions together should be sufficient to enable the first experimental studies of atom-molecule collisions in this temperature regime, and initial demonstrations of sympathetic cooling.

Our experimental setup for the RF MOT has been described elsewhere [15, 16, 18, 39]. In brief, pulses of SrF molecules are produced using a cryogenic buffer gas beam source [40, 41] and slowed with a "white light" scheme employing lasers $\mathcal{L}_{00}$, $\mathcal{L}_{10}$ and $\mathcal{L}_{21}$ [42]. Here, $\mathcal{L}_{vv'}$ denotes a laser tuned to the $X\,^2\Sigma^+\,|v, N^P = 1^-\rangle \to A\,^2\Pi_{1/2}\,|v', J'^{P'} = 1/2^+\rangle$ transition, where v is the vibrational quantum number, N is the angular momentum excluding spin, $\vec{J} = \vec{N} + \vec{S}$ (where $S = 1/2$ is the electron spin), P is the parity, and prime indicates the excited state. Except when the $\mathcal{L}_{vv'}$ notation is used, $v = v' = 0$ for all states relevant in this work. Slow molecules are captured in the RF MOT [16]. RF sidebands are added to each of the MOT lasers to address the resolved spin-rotation/hyperfine (SR/HF) structure in the SrF ground state. We use the most abundant isotopologue ^{88}Sr^{19}F, with nuclear spin 0 for ^{88}Sr and $I = 1/2$ for ^{19}F. Molecular laser cooling uses type-II cycling transitions ($F \to F' = F$ or $F - 1$, where $\vec{F} = \vec{J} + \vec{I}$

is the total angular momentum) [15], where there exist ground-state sublevels not optically coupled to the excited state (i.e., dark states) for any fixed laser polarization [43, 44]. The RF MOT destabilizes these dark states by rapidly and synchronously reversing the trapping laser polarizations and the MOT B-field gradient [45]. More details on the RF MOT and the level structure of SrF are given in the Supplemental Material [46].

We define the time of the ablation laser pulse that initiates a molecular beam pulse as $t = 0$. To load the RF MOT, we apply the slowing lasers from $t = 0$–35 ms and the trapping lasers, at maximum intensity, from $t = 0$–67 ms. Captured molecules are cooled and compressed by simultaneously reducing the trapping laser intensity from $t = 67$–117 ms and increasing the amplitude of the RF B-field gradient by $2\times$ [18]. The laser intensity and gradient amplitude are then held at their new values for 20 ms. We choose the final trap laser intensity to produce clouds with maximum density (as opposed to maximum PSD, as in our previous work [18]). Here, a final intensity 5% of the maximum value produces clouds at 1.1(1) mK, with density $1.8\times$ greater than when optimized for PSD.

Next, we apply sub-Doppler cooling, using a blue-detuned molasses similar to that recently demonstrated for CaF molecules [17]. At $t = 137$ ms, the RF MOT B-field gradient and polarization switching are switched off. The trapping light is extinguished for 0.1 ms as the trapping laser frequencies are jumped up by $+4.2\Gamma$ from the trapping values (where $\Gamma = 2\pi \times 6.6$ MHz is the natural linewidth); this produces a blue-detuned molasses with detuning $\approx +2.8\Gamma$ for each SR/HF level. The trapping light is then restored and applied to the molecules for 1.8 ms. During the molasses, three orthogonal shim coils, centered on the trapping region, are switched on to produce small, tunable B-fields. After the molasses, the trapping lasers are extinguished, and their frequencies are returned to the original values used in the RF MOT for subsequent laser-induced fluorescence (LIF) detection of the molecular cloud.

To probe properties of the molecular cloud, including molecule number and temperature, we use standard TOF fluorescence imaging [18]. We apply all MOT lasers at their full intensities (but without the RF MOT B-field gradient) to image the cloud on a CCD camera. In the case of magnetic trapping, the current in the trapping coils is fully switched off within 1 ms (see Supplemental Material [46]), during which time the molecular cloud expands negligibly, and we probe only after a time of flight of ≥ 3 ms (when eddy currents from the field switch-off have decayed to a negligible level).

Molasses settings were optimized to produce clouds with minimum temperature (Fig. 1). We find that optimal 3D sub-Doppler cooling in SrF requires careful control of the B-field, proper alignment of the MOT laser beams, and an optimized trapping laser intensity (found to be ≈ 60 mW/cm^2). (All laser intensities reported are
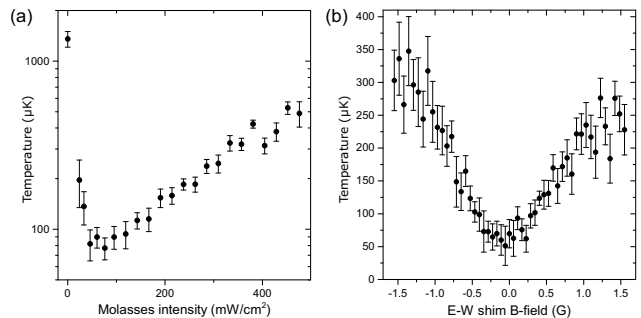
FIG. 1. Sub-Doppler cooling: (a) Molecular temperature after molasses vs. molasses laser intensity. The 0 mW/cm^2 point indicates the initial cloud temperature. (b) Molecular temperature after molasses vs. east-west shim coil B-field. Temperature dependence on north-south and up-down shim coil B-fields is similar (see Supplemental Material [46]).

averages over the $1/e^2$ area of the laser beams and, for the trapping lasers, summed over all six beams that form the arms of the MOT.) Our empirically-determined optimum B-field approximately cancels Earth's field in our laboratory. The optimized molasses cools molecules to temperatures as low as $T_{\mathrm{mol}} = 50(10)$ μK, with negligible loss in number. This temperature is $\approx 3\times$ smaller than the Doppler temperature, $T_{\mathrm{D}} = \hbar\Gamma/(2k_{\mathrm{B}}) = 160$ μK, and $\approx 5\times$ smaller than our previous lowest temperature [18].

To optimize the efficiency of capture in the MQT, molecules are next optically pumped towards the $|1; 3/2; 2; m = +2\rangle$ stretched-state Zeeman sublevel (where m is the projection of F, and we introduce the abbreviated state notation $|N; J; F; [m]\rangle$, where [ ] means m is not always specified), by driving transitions on all SR/HF lines of the $|N = 1\rangle \rightarrow |J' = 1/2\rangle$ resonance. This stretched state provides the maximum magnetic confinement available in $X\,^2\Sigma^+\,|N = 1\rangle$. (Approximately the same confinement is also achieved in one other state, $|1; 3/2; 1; m = +1\rangle$.) To achieve the OP, a π-polarized laser beam, with intensity ~ 16 mW/cm^2, and a σ^+-polarized laser beam, with intensity ~ 0.3 mW/cm^2, are applied simultaneously from $t = 140$–142 ms. The laser is tuned to the field-free resonance. The shim coil currents are rapidly set to provide a ≈ 6 G quantizing field, maintained until 1 ms after trap switch-on.

At $t = 142$ ms, the OP light is switched off, and the MQT is rapidly switched on in 250 μs, to an axial (vertical) gradient of 32 G/cm. This is above the levitation gradient for $|1; 3/2; 2; m = +2\rangle$ of 19 G/cm. The gradient can then be increased to a value as large as 140 G/cm over the next 100 ms to spatially compress the trapped cloud. The 3.6 mH inductance of our MQT coils makes rapid changes in current technically challenging. We use driving circuitry based on the designs in Ref. [47] (see the Supplemental Material [46]).

Despite the OP, substantial population remains in undesired sublevels at the time the trap is switched

on. The switch-on gradient is sufficient to levitate and confine only the two most strongly-trapped states, $|1; 3/2; 2; m = +2\rangle$ and $|1; 3/2; 1; m = +1\rangle$. However, if the gradient increases sufficiently rapidly during compression, some molecules in the other trappable states, including $|1; 3/2; 2; m = +1\rangle$ and $|1; 3/2; 1; m = 0\rangle$, will be trapped. We find it useful to analyze state populations in the MQT under two conditions: first, with the MQT maintained approximately at its switch-on gradient for the duration of trapping, so that only molecules in the two most strongly-trapped states are retained (referred to as the low-gradient case); and second, with the MQT gradient increased as rapidly as possible to its maximum value (referred to as the compressed case). In the low-gradient case, we load $\eta_{\text{low}} = 51(6)\%$ of the molecules in the MOT into the MQT. In the compressed case, $\eta_{\text{com}} = 80(4)\%$, $1.6\times$ larger. This indicates that, even with OP applied, $(\eta_{\text{com}} - \eta_{\text{low}})/\eta_{\text{com}} \approx 36\%$ of molecules remain in relatively weakly-trapped states in the compressed MQT. We also note, in passing, the importance of using both pre-cooling and OP to realize efficient transfer into the MQT: when only the optical molasses is applied, $\eta_{\text{com}} \approx 40\%$, while when neither molasses nor OP is applied, $\eta_{\text{com}} \approx 20\%$.

To further probe the $|F, m\rangle$ state distribution within the MQT, we use microwave spectroscopy. In particular, we monitor trap loss while driving transitions between various SR/HF levels of the $N = 1$ and $N = 0$ states, at ~ 15 GHz. This spectroscopy is performed for both the low-gradient and compressed cases (Fig. 2). A single microwave frequency (with intensity ~ 0.3 mW/cm^2 and broadened with uniform noise to 5 MHz or 10 MHz in the low-gradient or compressed case, respectively) is applied for 200 ms, starting 100 ms after the trap is switched on. The trap is then switched off, and the number of remaining $|N = 1\rangle$ molecules is measured as a function of microwave frequency.

Loss of signal from molecules in the target $|1; 3/2; 2; m = +2\rangle$ sublevel occurs when these molecules are driven to the $|0; 1/2; 1; m = +1\rangle$ sublevel. Since both these sublevels have the same magnetic moment, all trapped molecules in the target sublevel are resonant for the same frequency, 15.01 GHz, regardless of their energy in the Boltzmann distribution. This resonance produces a sharp, central loss feature in our data. (Molecules in $|0; 1/2; 1; m = +1\rangle$ remain trapped, but are not detected; moreover, molecules driven to this level can be re-excited to the untrapped $|1; 3/2; 2; m = 0\rangle$ level when they approach the field zero at the trap center.) Smaller features on either side of the central peak are associated with population in other sublevels. In the low-gradient case, the sum of the peak losses from the only two trapped states is consistent with 100%, indicating that microwaves can entirely deplete population in each trapped state under these conditions. Hence, the depth of the central loss feature indicates that a
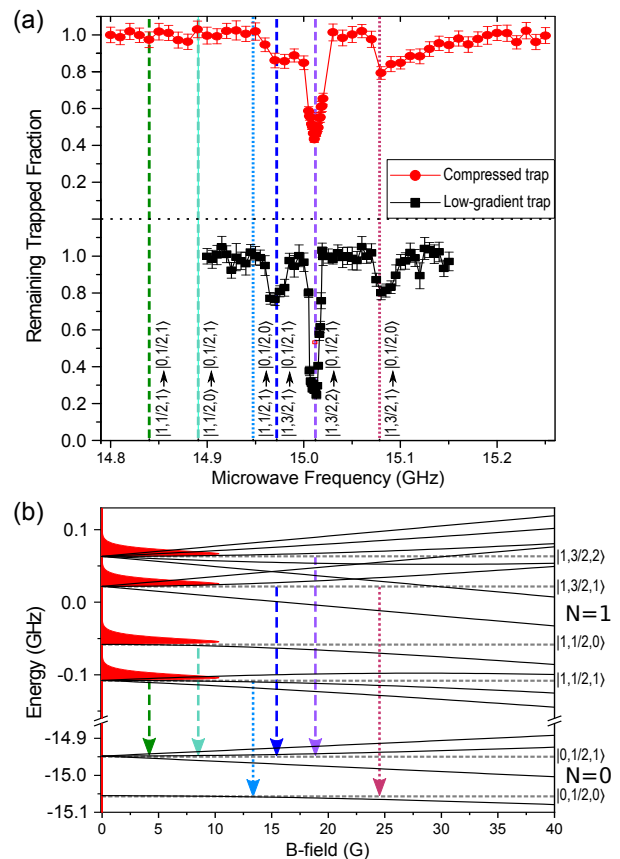
FIG. 2. (color online) Molecular state distribution in the MQT: (a) Microwave spectroscopy in the compressed (red circles) and low-gradient (black squares) MQT shows trap loss at frequencies corresponding to the $|1; 3/2; 1\rangle$ and $|1; 3/2; 2\rangle$ states. In the low-gradient case, the depth of the central loss feature indicates that $\approx 75\%$ of trapped molecules are in $|1; 3/2; 2; m = +2\rangle$. Dashed (dotted) lines mark the field-free frequencies of microwave transitions to $|0; 1/2; 1\rangle$ (to $|0; 1/2; 0\rangle$), as illustrated in plot (b). Error bars show the standard error of multiple measurements. Lines between points are a guide to the eye. (b) Breit-Rabi diagram for $X^2\Sigma^+$ $|N = 1; J = 1/2, 3/2\rangle$ and $|N = 0, J = 1/2\rangle$. Vertical arrows mark the six available microwave transitions, aligned below the relevant frequencies in plot (a). Red shaded regions show the energy spread for molecules in each trapped state, for a Boltzmann distribution at 260 μK.

fraction $f_{\text{m}=2} = 74(2)\%$ of molecules are in the target sublevel, with the balance in $|1; 3/2; 1; m = +1\rangle$, for the low-gradient case. In the compressed case, the decreased depth of the central loss feature likely reflects molecules populating additional trappable states such as $|1; 3/2; 2; m = +1\rangle$ or $|1; 3/2; 1; m = 0\rangle$. (We detect no clear evidence of molecules trapped in $|1; 1/2; 0, 1\rangle$ in the compressed case.)

From these measurements, we conclude that in the low-gradient case, $\eta_{\text{low}}^{m=2} = \eta_{\text{low}} \cdot f_{\text{m}=2} = 38(5)\%$ of molecules present in the RF MOT are loaded into the target

$|1; 3/2; 2; m = +2\rangle$ sublevel and magnetically trapped. This loading efficiency is comparable to efficiencies realized in experiments using ultracold atomic gases with closely-spaced transitions [48], as is the case for SrF where the splitting between $|1; 3/2; 1\rangle$ and $|1; 3/2; 2\rangle$ is only $\approx 6\Gamma$. The data also indicate that trapped molecules in the undesired $|1; 3/2; 1; m = +1\rangle$ state can be selectively and completely depleted, achieving a pure sample in the low-gradient case.

Next we discuss the temperature of molecules in the MQT, T_{MQT}. We first consider only molecules in the most strongly-trapped states. In the low-gradient case, only slight heating (to $T_{\mathrm{MQT}} \approx 90~\mu\mathrm{K}$) is expected based on an analytic expression for the energy imparted by the switch-on of the MQT [49]; we confirm this expectation in numerical simulations including the effect of gravity. We measure a temperature $T_{\mathrm{MQT}} \approx 80~\mu\mathrm{K}$ for this low-gradient case, in good agreement with the expected value.

For adiabatic compression in an MQT, $T_{\mathrm{MQT}} \propto G^{2/3}$, where G is the final gradient [50]. Under our conditions, the gradient increases by $\approx 4\times$ during compression, corresponding to a $\approx 2.5\times$ increase in T_{MQT}. Hence, considering only the most strongly-trapped molecules, we expect $T_{\mathrm{MQT}} \approx 230~\mu\mathrm{K}$ after compression. For a more realistic estimate, we perform a numerical simulation for an ensemble with 36% of molecules in states with half the magnetic moment of the strongly-trapped states. Applying our standard analysis to clouds from this simulation yields the apparent value $T_{\mathrm{MQT}} \approx 300~\mu\mathrm{K}$. In the compressed MQT, we measure $T_{\mathrm{MQT}} \approx 260~\mu\mathrm{K}$, in fair agreement with expectations from both these approaches. While the adiabaticity criterion is not well-satisfied early in our compression sequence (see Supplemental Material [46]), we see no clear evidence of heating in our simulations when comparing our compression ramp to a slower ramp.

In this work, no attempt has been made to maximize the number of molecules captured in the RF MOT. We typically observe $N_{\mathrm{MQT}}^{\mathrm{m=2}} \approx 600\text{--}800$ molecules in a single quantum state in the low-gradient MQT. In the compressed MQT, we measure a peak density $n_0^{\mathrm{all}} \approx 7 \times 10^4~\mathrm{cm}^{-3}$ for molecules in all states and infer a single-state peak density $n_0^{\mathrm{m=2}} = n_0^{\mathrm{all}} \cdot \eta_{\mathrm{low}}^{\mathrm{m=2}}/\eta_{\mathrm{com}} \approx 3 \times 10^4~\mathrm{cm}^{-3}$ (see Supplemental Material [46]). However, based on the loading efficiencies achieved here and the maximum number of molecules previously observed in our RF MOT, $N_{\mathrm{MOT}}^{\mathrm{max}} \approx 10^4$ [18], we expect that optimization could allow capture of $\approx 4 \times 10^3$ molecules in a single quantum state, with density $\approx 2 \times 10^5~\mathrm{cm}^{-3}$, in the MQT (see Supplemental Material [46]).

The MQT lifetime, τ_{MQT}, is measured by detecting LIF from the imaged cloud as a function of trap duration. Initial measurements in the compressed MQT gave $\tau_{\mathrm{MQT}} \approx 400\text{--}500$ ms, comparable to the maximum lifetime in our RF MOT [16]. This suggested that the loss was dominated by collisions with background gas for both
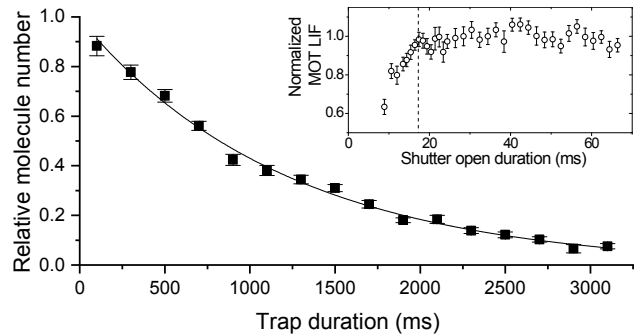
FIG. 3. Lifetime of molecules in the compressed MQT. Inset: MOT LIF signal vs. in-vacuum shutter open duration, Δt. Setting $\Delta t \geq 17$ ms (dashed line) yields optimal loading of the MOT. Main plot: with $\Delta t = 17$ ms, we measure $\tau_{\mathrm{MQT}} = 1.21(9)$ s. Error bars show the standard error of multiple measurements; line is an exponential fit.

the MQT and the MOT.

To increase the MQT lifetime, an in-vacuum shutter was added to the molecular beam line, to reduce the helium gas load from the cryogenic source (Fig. 3). This shutter, located 1.2 m upstream from the RF MOT, is open from $t = 0$ to Δt. With $\Delta t = 17$ ms, we measure an increased lifetime $\tau_{\mathrm{MQT}} = 1.21(9)$ s while leaving N_{MQT} unchanged. With the experiment repetition rates used here (0.3–1.4 Hz), this shutter duty cycle reduces the helium background pressure by $\sim 5\times$, down to a level similar to the total pressure of all other background gases.

At present, the in-trap molecule density is far too low to detect inelastic molecule-molecule collisions, while the trap depth is large compared to the temperature for all relevant conditions. Therefore, τ_{MQT} is expected to be independent of the B-field gradient. To confirm this, we also measure the lifetime in the low-gradient case and find $\tau_{\mathrm{MQT}} = 1.3(2)$ s. This is, as expected, negligibly different from τ_{MQT} in the compressed trap.

In summary, we have demonstrated efficient transfer of ultracold molecules from an RF MOT into an MQT. Our scheme is similar to those employed in experiments using ultracold atoms and achieves a transfer efficiency of $\approx 40\%$ into a single quantum state. Improvements to the apparatus are expected to allow compression of a pure sample, by applying microwaves to deplete molecules in $|1; 3/2; 1; m = +1\rangle$ and delaying compression until untrapped molecules have escaped the trapping region. Given typical anticipated cross-sections for Rb-SrF collisions at the observed temperature [28, 29], co-loading Rb atoms at peak density $n_{\mathrm{Rb}} \sim 10^{10}~\mathrm{cm}^{-3}$ (as typically achieved [37, 51]) would allow several SrF-Rb collisions within our observed trap lifetime [21]. This would in turn enable experimental exploration of sympathetic cooling of molecules by co-trapped, ultracold atoms. In the longer term, the increasingly high PSD accessible in conservatively trapped samples of polar

molecules holds enormous promise for future generations of precision measurement experiments [5, 52, 53].

———————

* Present address: Department of Physics, University of Connecticut, 2152 Hillside Road, Unit 3046, Storrs, CT 06269-3046. Corresponding author: daniel.mccarron@uconn.edu.

[1] K. Ni, S. Ospelkaus, M. H. G. de Miranda, A. Pe'er, B. Neyenhuis, J. J. Zirbel, S. Kotochigova, P. S. Julienne, D. S. Jin, and J. Ye, Science **322**, 231 (2008).

[2] J. G. Danzl, M. J. Mark, E. Haller, M. Gustavsson, R. Hart, J. Aldegunde, J. Hutson, and H.-C. Nägerl, Nature Physics **6**, 265 (2010).

[3] K. Aikawa, D. Akamatsu, M. Hayashi, K. Oasa, J. Kobayashi, P. Naidon, T. Kishimoto, M. Ueda, and S. Inouye, Phys. Rev. Lett. **105**, 203001 (2010).

[4] T. Shimasaki, M. Bellos, C. D. Bruzewicz, Z. Lasner, and D. DeMille, Phys. Rev. A **91**, 021401 (2015).

[5] L. R. Hunter, S. K. Peck, A. S. Greenspon, S. S. Alam, and D. DeMille, Phys. Rev. A **85**, 012511 (2012).

[6] M. R. Tarbutt, B. E. Sauer, J. J. Hudson, and E. A. Hinds, New Journal of Physics **15**, 053034 (2013).

[7] E. Altuntaş, J. Ammon, S. B. Cahn, and D. DeMille, Phys. Rev. Lett. **120**, 142501 (2018).

[8] D. DeMille, Phys. Rev. Lett. **88**, 067901 (2002).

[9] P. Rabl, D. DeMille, J. M. Doyle, M. D. Lukin, R. J. Schoelkopf, and P. Zoller, Phys. Rev. Lett. **97**, 033003 (2006).

[10] A. André, D. DeMille, J. M. Doyle, M. D. Lukin, S. E. Maxwell, P. Rabl, R. J. Schoelkopf, and P. Zoller, Nature Phys. **2**, 636 (2006).

[11] A. Micheli, G. K. Brennen, and P. Zoller, Nature Physics **2**, 341 (2006).

[12] R. V. Krems, Phys. Chem. Chem. Phys. **10**, 4079 (2008).

[13] L. Carr, D. DeMille, R. Krems, and J. Ye, New J. Phys. **11**, 055049 (2009).

[14] E. S. Shuman, J. F. Barry, and D. DeMille, Nature **467**, 820 (2010).

[15] J. F. Barry, D. J. McCarron, E. N. Norrgard, M. H. Steinecker, and D. DeMille, Nature **512**, 286 (2014).

[16] E. B. Norrgard, D. J. McCarron, M. H. Steinecker, M. R. Tarbutt, and D. DeMille, Phys. Rev. Lett. **116**, 063004 (2016).

[17] S. Truppe, H. J. Williams, M. Hambach, L. Caldwell, N. J. Fitch, E. A. Hinds, B. E. Sauer, and M. R. Tarbutt, Nature Physics **13**, 1173 (2017).

[18] M. H. Steinecker, D. J. McCarron, Y. Zhu, and D. DeMille, ChemPhysChem **17**, 3664 (2016).

[19] L. Anderegg, B. L. Augenbraun, E. Chae, B. Hemmerling, N. R. Hutzler, A. Ravi, A. Collopy, J. Ye, W. Ketterle, and J. M. Doyle, Phys. Rev. Lett. **119**, 103201 (2017).

[20] C. J. Myatt, E. A. Burt, R. W. Ghrist, E. A. Cornell, and C. E. Wieman, Phys. Rev. Lett. **78**, 586 (1997).

[21] I. Bloch, M. Greiner, O. Mandel, T. W. Hänsch, and T. Esslinger, Phys. Rev. A **64**, 021402 (2001).

[22] J. D. Weinstein, R. deCarvalho, T. Guillet, B. Friedrich, and J. M. Doyle, Nature **395**, 148 (1998).

[23] H.-I. Lu, I. Kozyryev, B. Hemmerling, J. Piskorski, and J. M. Doyle, Phys. Rev. Lett. **112**, 113006 (2014).

[24] Y. Liu, M. Vashishta, P. Djuricanin, S. Zhou, W. Zhong, T. Mittertreiner, D. Carty, and T. Momose, Phys. Rev. Lett. **118**, 093201 (2017).

[25] M. Zeppenfeld, B. G. U. Englert, R. Glöckner, A. Prehn, M. Mielenz, C. Sommer, L. D. van Buuren, M. Motsch, and G. Rempe, Nature **491**, 570 (2012).

[26] B. C. Sawyer, B. L. Lev, E. R. Hudson, B. K. Stuhl, M. Lara, J. L. Bohn, and J. Ye, Phys. Rev. Lett. **98**, 253002 (2007).

[27] D. Reens, H. Wu, T. Langen, and J. Ye, Phys. Rev. A **96**, 063420 (2017).

[28] G. F. Gribakin and V. V. Flambaum, Phys. Rev. A **48**, 546 (1993).

[29] M. Morita, M. B. Kosicki, P. S. Żuchowski, and T. V. Tscherbul, ArXiv e-prints (2018), arXiv:1801.07978 [physics.atom-ph].

[30] A. O. G. Wallis, E. J. J. Longdon, P. S. Żuchowski, and J. M. Hutson, The European Physical Journal D **65**, 151 (2011).

[31] T. V. Tscherbul, J. Kłos, and A. A. Buchachenko, Phys. Rev. A **84**, 040701 (2011).

[32] J. Lim, M. D. Frye, J. M. Hutson, and M. R. Tarbutt, Phys. Rev. A **92**, 053419 (2015).

[33] M. Morita, J. Kłos, A. A. Buchachenko, and T. V. Tscherbul, Phys. Rev. A **95**, 063421 (2017).

[34] G. Modugno, G. Ferrari, G. Roati, R. J. Brecha, A. Simoni, and M. Inguscio, Science **294**, 1320 (2001).

[35] D. J. McCarron, *A Quantum Degenerate Mixture of* ^{87}Rb *and* ^{133}Cs, Ph.D. thesis, Durham University (2011).

[36] L. Wacker, N. B. Jørgensen, D. Birkmose, R. Horchani, W. Ertmer, C. Klempt, N. Winter, J. Sherson, and J. J. Arlt, Phys. Rev. A **92**, 053602 (2015).

[37] W. Petrich, M. H. Anderson, J. R. Ensher, and E. A. Cornell, Phys. Rev. Lett. **74**, 3352 (1995).

[38] W. Ketterle and N. J. V. Druten, Advances in Atomic Molecular and Optical Physics **37**, 181 (1996).

[39] D. J. McCarron, E. B. Norrgard, M. H. Steinecker, and D. DeMille, New Journal of Physics **17**, 035014 (2015).

[40] J. F. Barry, E. S. Shuman, and D. DeMille, Phys. Chem. Chem. Phys. **13**, 18936 (2011).

[41] N. R. Hutzler, H.-I. Lu, and J. M. Doyle, Chemical Reviews **112**, 4803 (2012).

[42] J. F. Barry, E. S. Shuman, E. B. Norrgard, and D. DeMille, Phys. Rev. Lett. **108**, 103002 (2012).

[43] M. D. Di Rosa, European Physical Journal D **31**, 395 (2004).

[44] B. K. Stuhl, B. C. Sawyer, D. Wang, and J. Ye, Phys. Rev. Lett. **101**, 243002 (2008).

[45] M. T. Hummon, M. Yeo, B. K. Stuhl, A. L. Collopy, Y. Xia, and J. Ye, Phys. Rev. Lett. **110**, 143001 (2013).

[46] See Supplemental Material at URL to be inserted for additional details on the RF MOT, the MQT, and the molasses.

[47] S. Aubin, M. H. T. Extavour, S. Myrskog, L. J. Leblanc, J. Estève, S. Singh, P. Scrutton, D. McKay, R. McKenzie, I. D. Leroux, A. Stummer, and J. H. Thywissen, Journal of Low Temperature Physics **140**, 377 (2005).

[48] K. M. R. van der Stam, E. D. van Ooijen, R. Meppelink, J. M. Vogels, and P. van der Straten, Review of Scientific Instruments **78**, 013102 (2007).

[49] S. P. Ram, S. R. Mishra, S. K. Tiwari, and H. S. Rawat, Journal of the Korean Physical Society **65**, 462 (2014).

[50] W. Ketterle, D. Durfee, and D. Stamper-Kurn, in *Bose-Einstein condensation in atomic gases, Proceedings of the International School of Physics "Enrico Fermi", Course CXL*, edited by M. Inguscio, S. Stringari, and C. Wieman (IOS Press, Amsterdam, 1999) pp. 67–176.

[51] E. W. Streed, A. P. Chikkatur, T. L. Gustavson, M. Boyd, Y. Torii, D. Schneble, G. K. Campbell, D. E. Pritchard, and W. Ketterle, Review of Scientific Instruments **77**, 023106 (2006).

[52] The ACME Collaboration, J. Baron, W. C. Campbell, D. DeMille, J. M. Doyle, G. Gabrielse, Y. V. Gurevich, P. W. Hess, N. R. Hutzler, E. Kirilov, I. Kozyryev, B. R. O'Leary, C. D. Panda, M. F. Parsons, E. S. Petrik, B. Spaun, A. C. Vutha, and A. D. West, Science **343**, 269 (2014).

[53] W. B. Cairncross, D. N. Gresh, M. Grau, K. C. Cossel, T. S. Roussy, Y. Ni, Y. Zhou, J. Ye, and E. A. Cornell, Phys. Rev. Lett. **119**, 153001 (2017).